Solar energy harnessed by Pb₃CdO₇ nanocomposite for degradation of colored pollutants

Dushyant Kumar Prajapati[1], Jinesh Menaria[2], Jeevan Kunwar Chouhan[3], Tejveer Singh Tanwer[4,] Shipra Bhardwaj[5]

[1,2,3,4,5]*Department of Chemistry, Government Meera Girls College, Mohanlal Sukhadia University, Udaipur 313 001, Rajasthan, India*

Abstract—Novel ternary Pb₃CdO₇ nanocomposite is prepared using the facile co-precipitation approach and is characterized. Further advanced analysis is done by DTA, TGA, PL, FL, and BET methods and are reported herein. DTA-TGA analysis suggest the stability of nanocomposite up to 400°C. BET analysis shows pore size ranging from 1.804 nm to 4.658 nm. Lower rate of electron-hole pair recombination is ascertained by FL analysis. Strong near-band-edge (NBE) and deep-level emissions (DLE) are observed in PL spectra, which are associated with extrinsic defects that serve as charge carrier trap centers, hence enhancing photocatalytic activity. The band gap is found to be 5.23 eV. XRD shows it to be a nanomaterial with an average crystal size of 44.51 nm. SEM pictures display an agglomerated rod and sheet-shaped morphology. A kinetic study is conducted to determine the ideal degradation parameters, which include pH, dye concentration, photocatalyst quantity and light intensity for pollutants azure A (AA), erythrosine B (EB), and congo red (CR) where the results show degradation efficiency of 94.87%, 99.07% and 91.96% respectively. The quenching experiment verifies the participation of superoxide and hydroxyl radicals. The experiments suggest that it can be used up to five times without losing effectiveness. Laboratory tests are used to determine the final products and a mechanism is proposed as well.

Index Terms—Photocatalysis, solar energy trap, synthesis, characterization, first order kinetics

Graphical abstract
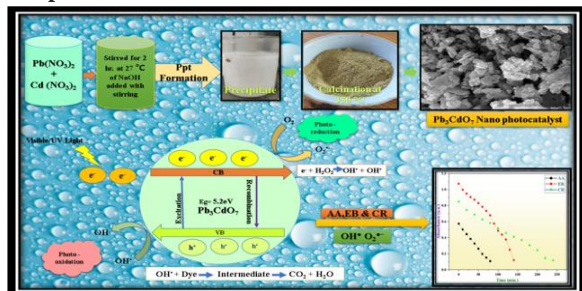
I. INTRODUCTION

It is well known that the textile industry produces a significant amount of wastewater that is contaminated with harmful chemicals and non-fixed dyes. The World Bank estimates that the textile processing industries are responsible for 17–20% of industrial water contamination. Different synthetic pollutants in water decrease the oxygen content causing serious health issues and so drew the attention of the researchers. Traditional techniques such as adsorption, coagulation, ion flotation, membrane process, sedimentation, etc. are still used to clean up contaminated water. Researchers are searching for low-cost and appropriate technology as wastewater treatment and recycling are major concerns. Heterogeneous catalytic methods have garnered greater interest in this context. Nearly total breakdown of contaminants can be accomplished even at mild pressure and temperature levels. This process's cost-effectiveness is one of its most important aspects.

The use of metal oxides as photocatalysts for dye wastewater treatment using nanoparticles was studied[1,2]. An article was published on recent advances in heterogeneous photocatalytic decolorization of synthetic dyes[3]. Bismuth oxychloride/titanium dioxide hybrid particles were used as heterogeneous photocatalysts by Liu *et al.*[4] for the same. The results indicated that BiOCl/TiO₂ showed enhanced photocatalytic performance under UV irradiation, and 50% BiOCl/TiO₂ exhibited the best photoactivity due to its high degree of crystallization, the mesoporous structure and corresponding large surface area, improved absorption ability in the UV region, and the

heterojunction formed between two coupling particles.

Synthesis of Ag-PbMoO$_4$ photocatalysts by facile sonochemical method with different molar% of Ag nanoparticles dispersed on the surface of PbMoO$_4$ was carried and Photocatalytic activities of them were evaluated under simulated solar light irradiation. The sample containing 0.3 mol.% of Ag showed the best photocatalytic activity[5]. Sahu et al.[6] prepared a series of Ti^{4+} containing ZnAl-LDHs with varying Zn:Al: Ti (~3:1:0–3:0.5:0.5) ratios and characterized them by various physicochemical methods like XRD, BET, TEM, etc. The derived mixed oxides from titanium-containing LDH precursors demonstrated better activity toward the photodegradation of methylene blue and rhodamine B than those of a physical mixture of ZnO and TiO$_2$. A visible-light-responsive MgO/ZnO/In$_2$O$_3$ mixed-metal oxide (MZI-MMO) hetero-structured photocatalyst was derived from a Mg-containing ternary hydrotalcite-like precursor followed by controllable calcination by Xiang et al.[7]. The kinetic studies suggested that the degradation of dye by MZI-MMO complies with a pseudo-first-order kinetic behavior.

Ternary zinc spinel oxides such as Zn$_2$SnO$_4$, ZnAl$_2$O$_4$, and ZnFe$_2$O$_4$ were synthesized by hydrothermal, metal–chitosan complexation, and solvothermal routes, respectively[8]. The mineralization degree of phenol molecules by Zn$_2$SnO$_4$ photocatalyst determined by total organic carbon analysis (TOC) reached 80% at 360 min under sunlight. Ullah et al.[9] synthesized ternary metal oxide nanophotocatalyst aluminum zinc ferrite (Al1-xZnxFe$_2$O$_4$). Its photocatalytic activity was evaluated by degrading reactive black B dye under sunlight irradiation with the help of a UV-visible spectrophotometer. The observed photo degradation rate was 91% in 120 minutes. A series of metallic silver and graphene (GR) co-doped monoclinic BiVO$_4$ ternary systems (Ag/GR/BiVO$_4$) were prepared by a single-step solvothermal method[10]. Their simulated sunlight and visible-light photocatalytic activity were evaluated by the degradation of a typical dye pollutant, rhodamine B (RhB). For comparison, binary systems of Ag/BiVO$_4$ and GR/BiVO$_4$ as well as solitary BiVO$_4$ were also tested under the same conditions. An enhanced photocatalytic activity for TiO$_2$–CdO composite for

hydrogen generation from aqueous solution of Na$_2$S + Na$_2$SO$_3$ compared to pure CdO and TiO$_2$ was studied[11]. Varied morphologies and compositions of bismuth tungstate nanocomposites were investigated as promising materials for photocatalytic applications[12]. The resulting Bi$_2$S$_3$/Bi$_2$WO$_6$ hetero-catalysts were used to remove toxic Cr(VI) ions via reduction to water-insoluble Cr(III) utilizing visible-light irradiation. A PVP-capped Cd and Ag-doped ZnO (Cd:Ag:ZnO:PVP) multifunctional nanocomposites was synthesized for photocatalytic applications by facile microwave-aided precipitation way[13]. The degradation rate of Cd:Ag:ZnO:PVP nanocomposite was 4.7 times higher than that of undoped ZnO for methylene blue (MB) dye. EIS responses show improved photocatalytic properties and more charge carrier ability due to the large surface area (94.51 cm^3 g^{-1}). A facile preparation of Cd$_2$SnO$_4$ microcrystals was carried out and the results confirm that cubic structure offers higher degradation ability for degradation of Rhodamine B dye as compared to orthorhombic Cd$_2$SnO$_4$ due to lower recombination of the electron-hole pairs, which is supported by PL spectra[14]. Haritho et al.[15] electro-deposited PbO$_2$ over ZnO-TiO$_2$ core-shell structure to alter its surface for electrocatalytic degradation of dye. The electrochemical and photocatalytic behaviors of the coatings were analyzed for the removal of RB-5 dye as a model pollutant.

Synthesis of rGO/CdO/SnO$_2$ ternary nanocomposite was carried out and the photocatalytic activity of the as-synthesized sample was measured against malachite green and congo red dyes. The higher percentage of CdO/SnO$_2$ in the rGO/CdO/SnO$_2$ showed maximum photocatalytic degradation[16]. Synthesis of novel hetero-structured ZnO-CdO-CuO nanocomposite was carried by Munawar et al.[17]. Ternary oxide NiO-CdO-ZnO nanocomposite along with pure NiO, CdO, and ZnO was also prepared by the homogeneous co-precipitation method. The photocatalytic activity of grown nanocomposite against rhodamine B and methylene blue dyes under sunlight revealed high degradation efficiency of 99% and 98% in 60- and 90-min illumination respectively[18]. The ternary nanocomposite ZnO–CdO–Pr$_2$O$_3$ (5 mg/l) showed 93% degradation efficiency. The adsorption kinetic of dyes on the surface of the photocatalyst was effectively described by using a first-order kinetics model with all $R^2 > 95$

indicating the strong relationship between time and dye concentration. A possible schematic model was proposed to endorse the mechanism of degradation. Furthermore, species trapping experiments using various scavengers were conducted and results indicated that $O_2^{.-}$ and OH Radicals were actively involved in the degrading process[19]. Ternary $NiO/CdO/Co_3O_4$ nanocomposite powder was synthesized using the sol-gel method. The prepared sample was compared with a binary NiO/CdO composite for dye degradation under visible light irradiation[20].

Quaternary-based ZnO-PbO-CdO-CuO nanocomposite was synthesized by a feasible 'one-pot' chemical method[21]. The photocatalytic dye degradation activity of composite was evaluated by employing two model dyes namely, Fast Green and Rose Bengal under sunlight irradiation. Logambal *et al.* used PbO NPs for photocatalytic degradation of methylene blue dye under UV irradiation[22]. Asha *et al.* studied the photocatalytic activity of the prepared nanoparticles $PbWO_4$ for degradation of textile wastewater under UV light irradiation. The photocatalytic reaction rate constant was found to be 0.014/min[23]. The photocatalytic behavior of the $CsPbI_3$ nanostructures was studied for the destruction of methyl violet, with a decolorization percentage of 81.7[(24)].

$Ho_2Ti_2O_7$ andchitosan-coated $Ho_2Ti_2O_7$ nanocomposites were prepared through a facile auto-combustion and co-precipitation route. Their photocatalytic performance was explored over several dyes as pollutants under visible radiation[25]. The incorporation of the non-ionic surfactant Triton X-100 blend with CuO/CdO resulted in hexagonal-shaped grains with a nanoporous structure showed photocatalytic activity against Rhodamine-B (RhB) where a 94% degradation efficiency as compared to pristine CuO (71.42%) and CdO (77.83%) was observed. In acidic solution, the reusability of CuO/CdO was observed outstanding with a 95.80% degradation efficiency after five successive cycles[26]. Monsef *et al.*[27] synthesized $PrVO_4$ nanoparticles and $PrVO_4$/ CdO nanocomposite to improve photocatalytic efficiency. To obtain the desired sample, various amine sources were used as precipitating agents. Their photocatalytic activity was examined by the degradation of azo dyes under UV and visible irradiation. Warshagha *et al.*[28] used co-

precipitation method for synthesizing heterojunction nanocomposite (CdO-ZnO). Standard analytical techniques were used to characterize the synthesized composite. Under visible light irradiation, the as-prepared CdO-ZnO nanocomposite demonstrated very efficient photocatalytic performances for degradation of paracetamol, ciprofloxacin etc. in aqueous solutions. The photocatalytic process appeared to be dominated by OH free radical and h^+, according to the radical scavenger tests.

$CdTiO_2$ and $ZnCdTiO_2$ nanocomposites were prepared by co-precipitation method[29] and the band gap energy of TiO_2 (2.65) decreased to 2.6 and 2.56 eV for $CdTiO_2$ and $ZnCdTiO_2$, respectively. BET analysis showed a 47.2 m^2/g surface area for the ternary $ZnCdTiO_2$ nanocomposite. The photodegradation results revealed that TiO_2, $CdTiO_2$, and $ZnCdTiO_2$ degraded about 74%, 86%, and 97.61% methylene blue dye, respectively, within 2 h. Maximum photodegradation was achieved in the basic medium and the ternary $ZnCdTiO_2$ nanocomposite degraded 98% dye at pH 10. CdO–ZnO nanocomposite as a photocatalyst, for the degradation of Methylene blue, Rhodamine B, and Methyl orange dyes was prepared[29,30]. The results found enhanced dye degrading efficiency with cadmium oxide contents in composites as compared to bare ZnO nanostructure.

It was observed that ternary photocatalysts can bring wonders but were found less involved in removal of carcinogenic harmful organic materials from wastewater that too in heterolytic manner. Thus, an attempt is made in the present work to provide a facile route of synthesis and use of a novel, cheaper and efficient ternary nanocomposite for the removal of some carcinogenic dye from water so that water can be used further for various means.

II. MATERIALS AND METHODS

A. Materials

All the chemicals of analytical grade (> 99 %) are used without further purifications, including absolute ethanol (CH_3CH_2OH, 99.9%), sodium hydroxide pellets (NaOH, 96%, Merck Co. Ltd.). EDTA, ether, isopropyl alcohol, hydrochloric acid, isopropyl alcohol, potassium iodide, and benzoquinone (CDH). Distilled water is used throughout the experiments.

B Photocatalytic study

The photocatalytic activity of the Pb_3CdO_7 nanocomposite is evaluated for degradation of erythrosine B (EB, BDH), azure A (AA, BDH), and congo red (CR, BDH) dyes. The experiments are carried out in a borosil beaker covered by a water filter to avoid the effect of heat on the reaction mixture. The solution is exposed to a 250-watt tungsten filament lamp. The intensity of light is recorded by a solarimeter (New CHEM Dt 1307). the pH of the dye solutions is measured by a pH meter (Hena pen type) and is adjusted by pre-standardized NaOH and HCl solutions. The optical density of various solutions undergoing reaction is measured by a UV-visible spectrophotometer (CHINO).

C Characterization

An STA 6000 (Perkin Elmer) Build 36 differential thermal analyzer (TG-DTA) is used to measure the thermal stability under a nitrogen environment at a heating rate of $10°C$ min^{-1} from room temperature $25°C$ to $900°C$. Photoluminescence spectra (PL) is carried out at room temperature $25°C$ (F-7000, Hitachi, Japan). Using a 532nm laser source as the excitation source, Raman spectra are captured on a microscopic confocal Raman spectrometer. Brunauer– Emmett–Teller (BET) surface area of the sample is measured using N_2 adsorption at $77.35°K$ (Quanta chrome equipment). Fluorescence emission spectra (FL) is recorded on a 55 (Perkin Elmer) type fluorescence spectrophotometer over a wavelength range of 200–800nm. Using a Shimadzu Analysis - Elementar, Liqui TOC, the total organic carbon (TOC) content of the dye solutions is determined.

III. RESULTS AND DISCUSSION

A. Synthesis of Pb_3CdO_7 nanocomposite

Pb_3CdO_7 nanocomposite is prepared by its precursor nitrates. The co-precipitation method is shown schematically in Figure 1 and the yield obtained of prepared nanocomposite is 88% at pH 10. It is then thoroughly washed by distilled water several times, dried, calcined and characterized by various techniques.
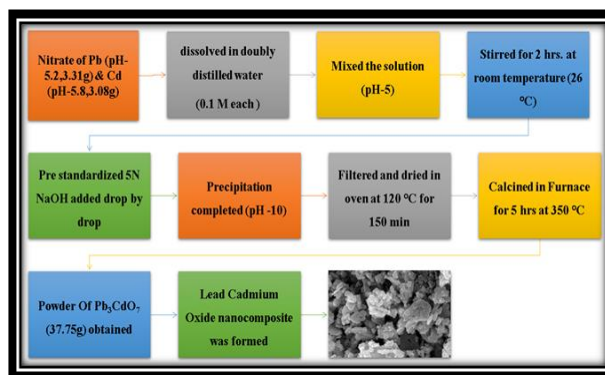
Fig. 1. Schematic representation of synthesis of Pb_3CdO_7 nanocomposite

B. Characterization

1 Photoluminescence spectroscopic analysis

The nature, density, and structural flaws occurring during the route of synthesis of the Pb_3CdO_7 are examined using PL spectroscopy. The data are represented graphically in Figure 4 and are supported by earlier studies[31,32]. The energy levels of the structural flaws are often understood to be responsible for visible light emission. For Pb_3CdO_7 with a band gap of 5.23 eV, theoretical calculations showed that Pb, Cd, and O are positioned below the conduction bond (CB) and above the valence bond (VB). A simple Gaussian fit of the PL curve for nanocrystals is illustrated by dotted curves in Figure 2. Two luminescence bands are observed, a broad UV-visible light band and a near UV band. A wide emission is seen at room temperature at an excitation wavelength (λ) of 128 nm, extending from UV to visible areas.

Five peaks are obtained as a result of the curve fitting. The peak centered at 135 nm (range 123-144 nm, 79.02%) stands for green emission, shows maximum absorbance, and may be attributed to the excitation of an electron from VB of filled 2p orbital of oxygen to the CB of empty 6p orbital of Pb. The peak centered at 150 nm (133-165 nm, 55.20%) is the yellow emission, and the peak centered at 182 (152 to 209 nm) stands for brown emission. The near band edge (NBE) transition caused by direct recombination of the electrons in the free excitation level and holes in the VB, is identified as the source of the UV emission at this emission. The peak centered at 250 nm (186-308 nm, 53.58%) depicts the orange emission, and the peak centered at 358 nm (281-410 nm, 35.63%) shows the grey emission. The

broad band at 358nm originates from the recombination of generated electrons and holes at the surface of the material[33]. Other peaks illustrate the transition between oxygen vacancies and defects. Shifts in the emission peaks towards the lower wavelength are due to the quantum confinement effects. It is also reported that lower intensity peaks of PL suggest that the photocatalytic activity of the nanoparticles is improved with the low recombination rate of the photo-generated electron-hole pairs. The defect-related blue emission peak is not observed due to reduced surface defects of CdO[34].
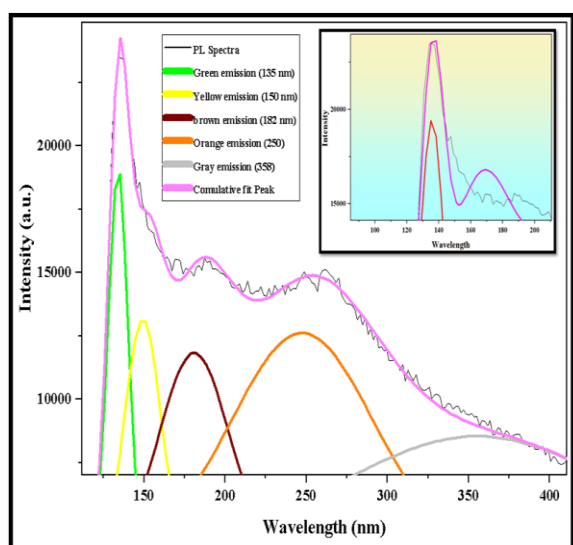
Fig. 2. Photoluminescence spectra of Pb_3CdO_7 nanocomposite

2 TGA and DTA analysis

The TGA and DTA analyses of the prepared Pb_3CdO_7 nanocomposite are performed in a static air environment between 0 and 900°C at a rising rate of 10°C/min to examine the crystalline nature of the synthesized nanocomposite after heat treatment and are shown in figure 3. The breakdown is shown by the drastic weight decrease after 400°C. Transition metal removal is responsible for the initial mass loss in the TGA between 250 and 600°C which is accompanied by an endothermic peak in the DTA curve. A strong exothermic peak was observed in the DTA curve, which is centered between 450 and 600°C and is linked to the crystallization of Pb_3CdO_7. The reduced stability of the nano-structures relative to the single crystal of the produced complex is confirmed by certain variations in the maximum

intensities in TGA data. Three distinct slopes of weight loss processes were observed at 364°C (1.19%), 381°C (1.85%) and 472°C (3.05%). A single endothermic peak at 423°C in the DTA curve is observed suggesting the transition phase which is responsible for the little weight loss that occurs in the third stage between 400 and 630°C. DTA finally allowed us to locate a single endothermic peak at 600°C. The curve aligned with the temperature axis beyond 660°C endorsed the stability of Pb_3CdO_7 nanoparticles.
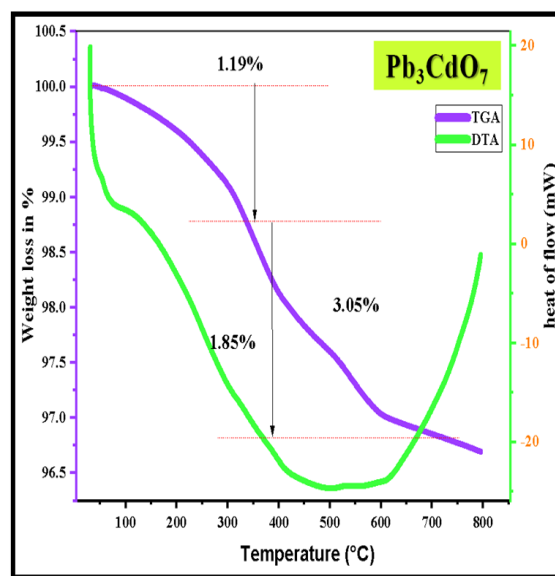
Fig. 3. TGA-DTA analysis of Pb_3CdO_7 nanocomposite

3 Brunauer-Emmett-Teller (BET) analysis

The Brunauer-Emmett-Teller (BET) analysis is a key analytical tool for determining the precise surface area of synthesized nanocomposites[35,36]. It seeks to explain the physical adsorption of gas molecules on a solid surface, pore size distribution, and nitrogen adsorption-desorption isotherms. As depicted in Figure 4 (a), (b), (c), Pb_3CdO_7 nanocomposite has a specific surface area of 9.243 m²/g in Langmuir data with pore size ranging from 1.804 nm to 4.658 nm. The isotherm curves show that the hysteresis loop lies between 0.65 and 0.80 of relative pressure (P/Po). BJH method Desorption (dV) shows the Surface Area = 7.643 m²/g, Pore Volume = 0.067 cc/g, Pore Diameter Dv (d) = 1.804 nm, Average pore diameter = 4.658 nm and total pore volume = 6.65 cc/g at P/Po = 0.993. MBET showed a surface area to be 5.712 m²/g.
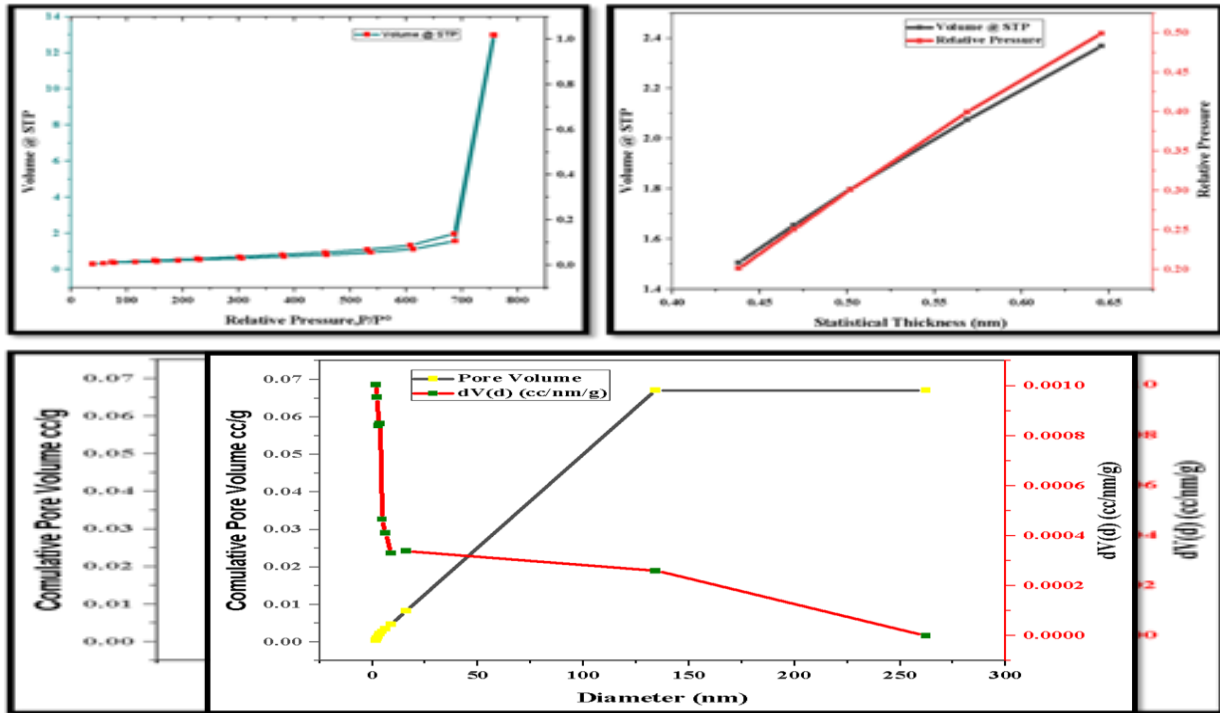
Fig.4. (a) raw data analysis (b) t-plot data (c) pore size distribution desorption (dv) data for Pb_3CdO_7 nanocomposite

4 Fluorescence spectroscopic analysis

The recombination of electrons and holes on a photocatalyst surface results in the release of energy in the form of emission[37]. Decreased electron-hole recombination rate is implied by lower fluorescence emission intensity. The detection spectra were acquired using an excitation wavelength of 200 nm in the 200-800 nm range at room temperature. It is evident from Figure 5 that nanostructured Pb_3CdO_7 has high emission peaks at 345.5 and 690 nm suggesting the photosensitive and photoactive nature of the Pb_3CdO_7 photocatalyst. TEM image and electron diffraction pattern of the photocatalyst are combined with the bandgap energy measurement using UV measurement techniques. It should be noted that these peaks correspond to the bandgap energy of 5.23 eV.
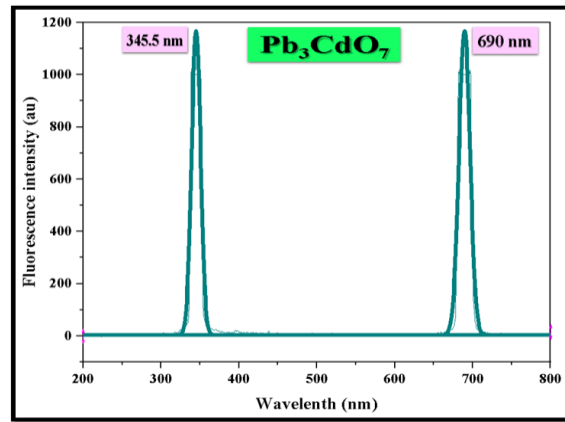
Fig.5. Fluorescence emission spectra of Pb_3CdO_7 nanocomposite

The XRD diffraction patterns, FESEM and HR-TEM images of Pb_3CdO_7 nanocomposite showed that it possesses a cubic crystalline shape with some two-dimensional sheet-type structure. EDX displayed the ratio for Pb, Cd, and O which appears to be 3.0:1.0:7.3 that accord well with the suggested formula Pb_3CdO_7. The average particle size was 44 nm suggesting the nanocrystalline nature of the synthesized composite. The optical bandgap (E_g) was calculated to be 5.23 eV suggests that the

nanocomposite exhibits excellent photocatalytic properties[38].

C. A Comparative Kinetic Study of the Degradation of Dyes:

Using spectrophotometry, the optical density of the experimental solution is examined at λ_{max} for AA, EB, and CR at 630, 520 and 490 nm respectively. 50 mL solution of each dye of a certain concentration is placed in a beaker, and the pH of the solution is adjusted using pre-standardized NaOH and HCl solutions. A particular amount of photocatalyst Pb_3CdO_7 is added to each solution and it is then exposed to the tungsten lamp. A water cutoff filter is applied to the solutions to avoid heat reactions. The sample is inspected at different time intervals by recording optical density.

1 A typical run

The graph between $1 + \log$ Optical density (O.D.) and time is drawn for each dye and it shows a straight line suggesting the reaction to follow pseudo-first order kinetic law. The resulting data are presented in Table 1 and a typical run is shown graphically in Figure 6. $k = 2{:}303 \times$ slope, is used to find the rate constant. At certain values of parameters (Table 1), the highest degradation rate constant observed for AA is 4.510×10^{-4} s^{-1}, for EB is 2.253×10^{-4} s$^{-1,}$ and for CR comes out to be 1.454×10^{-4} s^{-1}.
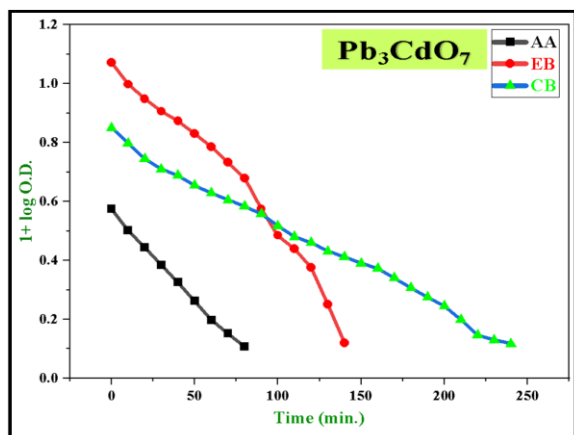
Fig.6. Typical run for photocatalytic degradation of AA, EB, and CR

2 Effect of pH on degradation of dyes

The primary component influencing dye degradation is pH of the solution. Changes in initial values of O.D. are attributed to the pH-sensitive nature of dyes. The effect of pH on the degradation of AA, EB, and CR is investigated by varying it in the range of 4 to 11 and by keeping all other variables constant. The experimental comparative results are graphically shown in Figure 7. The maximum rates of degradation are seen at pH 10.5, 10.0, and 6.5 for AA, EB, and CR, respectively.

The rate of reaction increases as pH is increased and can be explained by the fact that the concentration of OH$^-$ ions increases with an increase in pH. The generation of holes on the surface of the photocatalyst, on exposure to light, tends to abstract an electron from these ions, and OH$^\bullet$ free radicals are generated. Simultaneously $O_2^{\bullet-}$ superoxide anion radicals are also produced (refer mechanism). Attack of these free radicals (as confirmed by scavenger test) initiates break down of weaker bond sites at dye molecules causing degradation of them. The rate of reaction reduces after a limit as $O_2^{\bullet-}$ and OH$^\bullet$ free radicals now repel each other and the cationic surface of dyes as well. As a result, the pace of degradation falls.
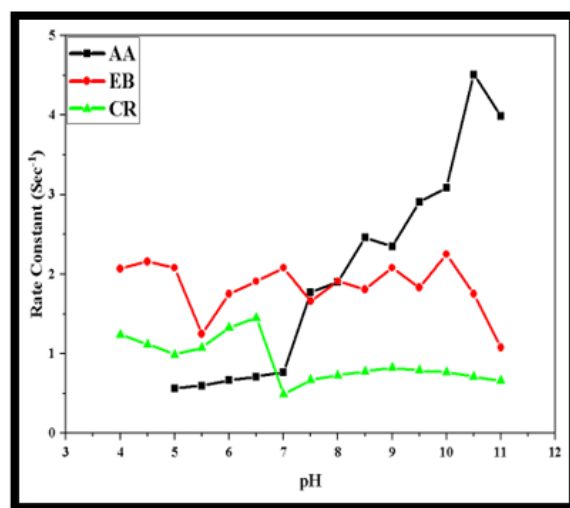
Fig. 7. Effect of pH

3 Effect of concentration of dye on degradation

Pollutant concentration is the main factor to be considered while treating wastewater. Thus, the impact of different concentrations of dyes on the degradation rate is considered and is depicted in Figure 8. All other factors are kept constant. The concentration is adjusted between 0.4 and 2.0×10^{-4} Moles Lit^{-1}; 0.4 and 2.0×10^{-4} Moles Lit^{-1} and 2.2 and 3.8×10^{-4} Moles Lit^{-1}; for AA, EB, and CR, respectively. It has been noted that as dye concentration rises, the rate of degradation increases.

This is because there are more dye molecules available absorb photons from light and to excite from ground to singlet state. After a certain limit, when dye concentration is increased, the molecules themselves start working as filters, preventing the required wavelength from reaching the surface of photocatalyst particles. Thus, the rate of degradation decreases.
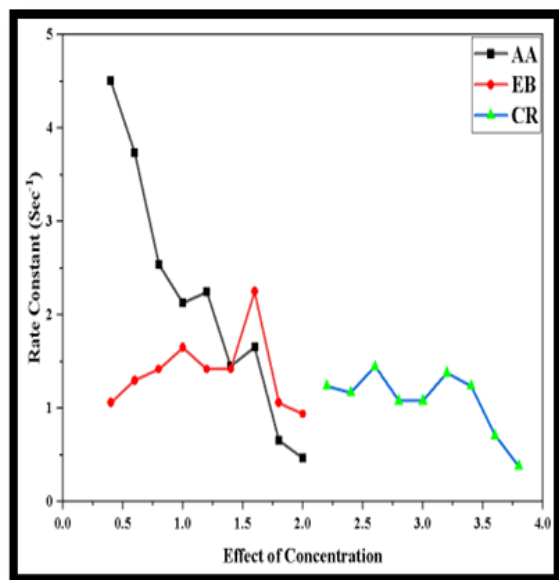
Fig. 8. Effect of concentration of dyes (moles Litre^{-1})

4 Effect of photocatalyst loading on the degradation of dyes

One of the factors influencing the rate of degradation of dye is the photocatalyst dose. Keeping all other parameters unchanged, it was changed from 0.04 to 0.20 g for AA, 0.04 to 0.22 g for EB, and 0.04 to 0.22 g for CR. The experimental results shown in Figure 9 suggest that adding more catalysts after a certain amount causes the catalyst particles to aggregate only further, once the respective maximum values are reached. The phenomenon may be explained by the fact that as the amount of photocatalyst rises, so does its surface area, which generates a higher number of hole-electron pairs at the catalyst's surface. As a result, more radicals are produced and the rate of degradation is accelerated. Beyond the maximum, adding more amount of photocatalyst produces more hole-electron pairs which forces the electron-hole recombination. Therefore, a decrease in the rate is noted.
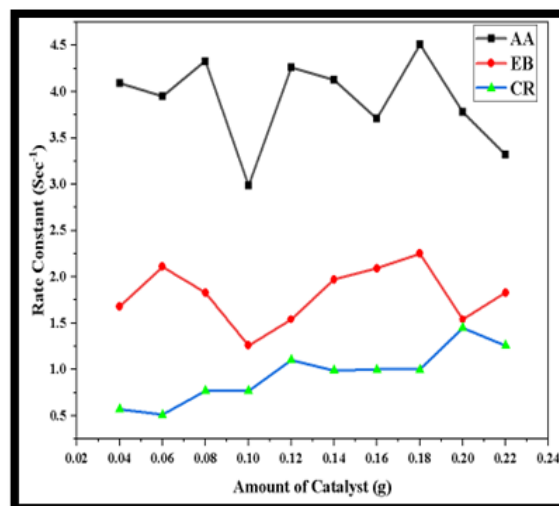
Fig. 9. Effect of photocatalyst loading (g)

5 Effect of intensity of light on the degradation of dye

The light intensity was varied from 506 to 1530 mWcm^{-2}, with keeping all other factors constant. The data for all three dyes is shown in Figure 10. It is observed that the rate of reaction increases with an increase in light intensity for all three dyes. It is attributed to the fact that a greater number of photons strike the photocatalyst surface generating a greater number of electron hole pairs. As a result, more dye molecules are stimulated which are responsible for degradation. Light intensities above 1530 mWcm^{-2} cause heat reactions and so are avoided.
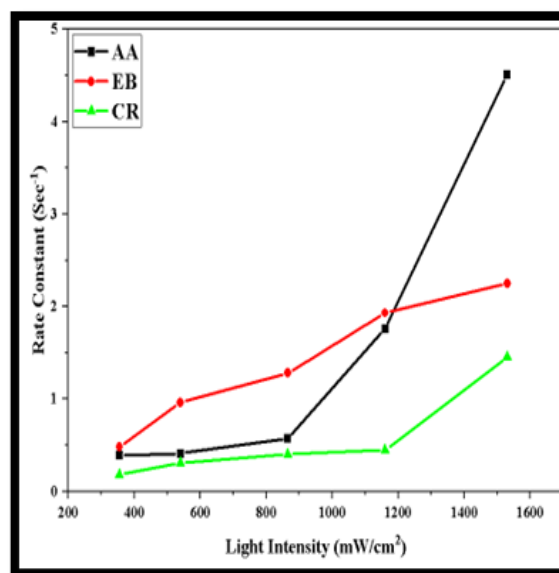
Fig.10. Effect of light intensity (mWcm^{-2})

6 Scavenger study

A scavenger test with various scavengers (EDTA, Isopropyl alcohol, KI, and Benzoquinone) is carried out to determine the active free radical species participating in the degradation process and for interpretation of the mechanism. It is observed that the reaction has ceased completely albeit with a minor deterioration, by EDTA (superoxide anion radical scavenger) for AA, by IPA (hydroxyl free radical scavenger) for EB and CR. It shows that $O_2^{\bullet-}$ for AA and $OH^{\bullet}$ for EB and CR, are the species responsible for photocatalytic degradation.

7 Recycle experiment

The recycle experiment illustrates the endurance of Pb_3CdO_7 for the degradation of AA, EB, and CR dyes in addition to its strong photocatalytic activity. No discernible drop-in photocatalytic activity was seen after five reuses, indicating the material's great stability and long-lasting activity under constant exposure to visible light. Nevertheless, the catalyst's degrading efficiency dropped from 99.07% to 84.08% after five reuses. The inorganic ions adsorbed on the Pb_3CdO_7 photocatalysts during the degradation may be the cause of the reduction in photocatalytic activity.

8. A Comparative Analysis

Table 1: Comparative data for degradation of dyes

S.No.	Resulting factors	AA	EB	CR
1.	Λ_{max} (nm)	630	520	490
2.	Conc. of Dye x 10^{-5} (moles L^{-1})	4.00	1.60	2.60
3.	pH	10.5	10.0	6.5
4.	Amount of Nanocomposite (g)	0.08	0.18	0.20
5.	Intensity of Light (mWcm^{-2})	1530	1530	1530
6.	Degradation time (min.)	40.00	160.0	240.0
7.	Degradation%	94.87	99.07	91.96
8.	Rate constant × 10^{-4} (Sec^{-1})	4.510	2.253	1.453
9.	Total Organic Carbon (mgL^{-1})	4.591	7.507	8.050

The presence of heteroatom in the ring in AA makes it polar and thus attack of free radicals is facilitated to break it into fractions. Ring strain in aryl groups is dispersed throughout the structure of EB, making bond breakdown in it simpler. Compared to the other dyes, CR is a bulkier molecule that takes a longer span to degrade. Hence, the following sequence of rate of deterioration is ruled out: AA >EB > CR.

1 Mechanism:

After examining the effects of several variables on the degradation of all three dyes, it is contemplated that AA degrades more quickly than EB and CR. Chemical structures, bond strengths, and the impact of ring strain on dye molecules are used to explain this. The following relation was used to compute the degradation efficiency:

Degradation efficiency = $[(C_0 - C_t)/C_0] \times 100\%$

Where C_0 is the initial concentration and C_t is the concentration (mgL^{-1}) after irradiation at different time intervals. When exposed to light, the photocatalytic performance of the Pb_3CdO_7 nanocomposite is well observed for AA, EB, and CR where 94.87%, 99.07%, and 91.96% are destroyed after 40 minutes, 160 minutes and 240 minutes of exposure, respectively. The maximum degradation conditions are extracted from experiments for all three dyes and are tabulated in Table 1. Total organic carbon (TOC) is also determined experimentally after photocatalytic treatment of the dye solutions and it is found to be 4.591 mgL^{-1} in AA, 7.507 mgL^{-1} in EB, and 8.050 mgL^{-1} in CR dye solution which is within the permissible limit.

A possible mechanism based on experimental data for the degradation of AA and EB, CR dyes in the presence of Pb_3CdO_7 composite has been suggested:

(1) $_1Dye^0 + h\upsilon \rightarrow {}_1Dye^1$ (Excitation from ground state)
(2) $_1Dye^1 + h\upsilon \rightarrow {}_1Dye^3$ (ISC)
(3) $Pb_3CdO_7 + h\upsilon \rightarrow Pb_3CdO_7 [e^- (CB) + h^+ (VB)]$
(4) $e^- + O_2 \rightarrow O_2^{\bullet-}$ (Superoxide anion radical)
(5) $h^+ + H_2O \rightarrow OH^{\bullet} + H^+$ (Hydroxyl radical)

(6) AA + $O_2^{\bullet-}$ → degradation products NO_2, CO_2, H_2O etc.

(7) EB & CR + $OH^{\bullet}$ → degradation products NO_2, CO_2, H_2O etc.

2 Determination of fragmentation by LCMS/MS analysis:

The LCMS/MS approach is used to identify the process of degradation of erythrosine B dye. This analytical technique analyses the fragmentation of any molecule to determine its structure. The XEVO-G2S-Qtof instrument waters with ESI type, source temperature of 144°C, mass range of 125 to 1000, duration of 15 minutes, and collision energy of 3.0 are used for the analysis.

To determine the tentative breakdown and potential degradation route, the values of m/z were computed. The dye solution with pH 10.5, 0.18 g of photocatalyst, and a dye concentration of 0.4×10^{-4} M, was exposed to 1530 mW/cm^2 of light. Five samples, each around 10 mL in volume, were taken at 40, 80, 120, 160 and 180-minute intervals, and LCMS analysis was performed. Figure 11 provides the data of different m/z peaks.

Sample drawn at 40 minutes
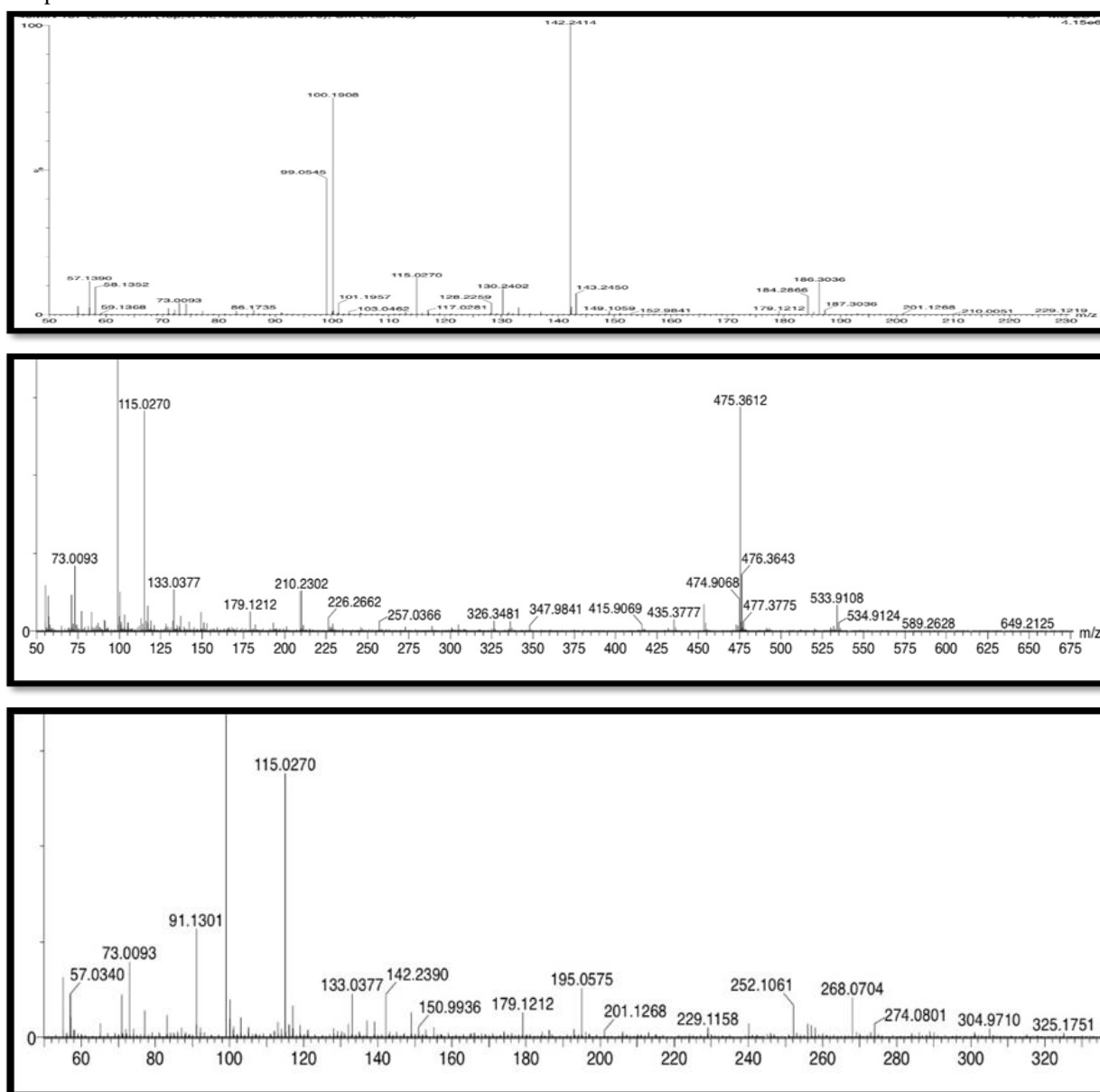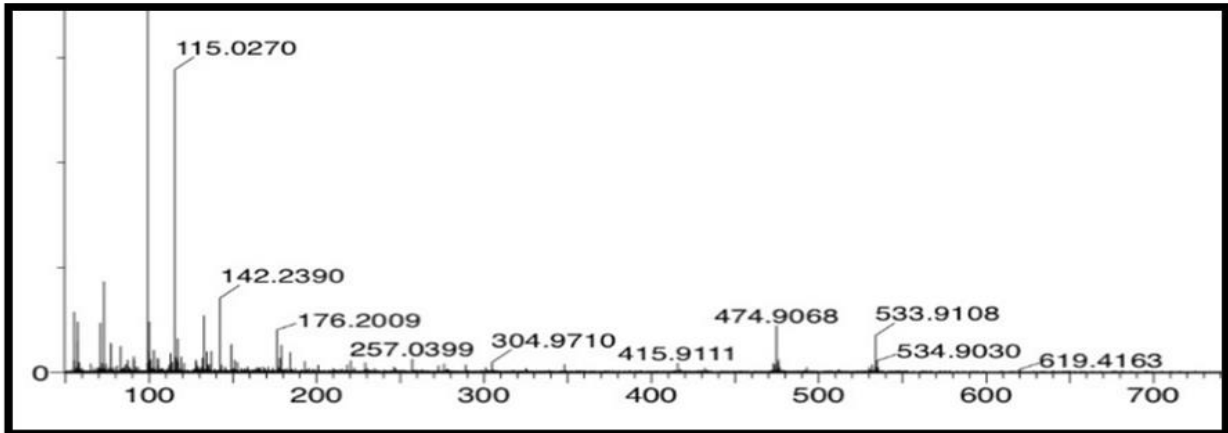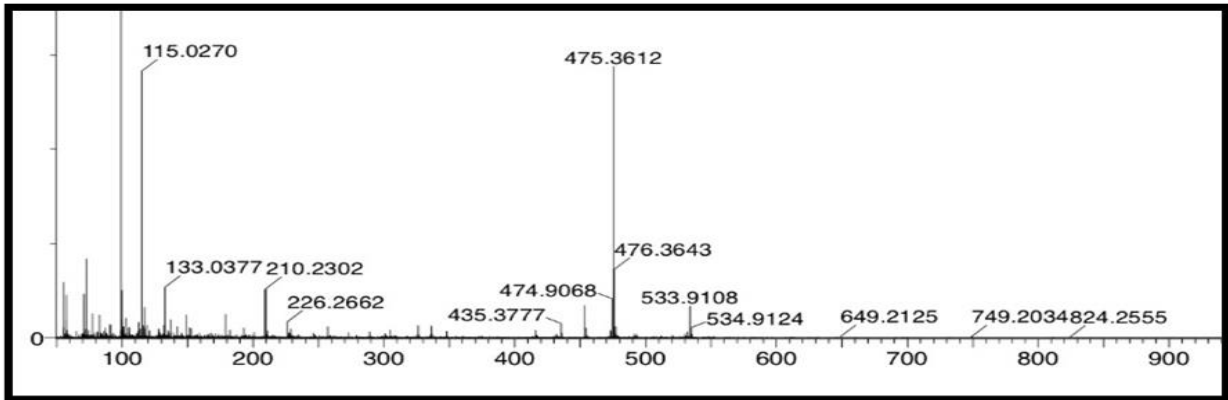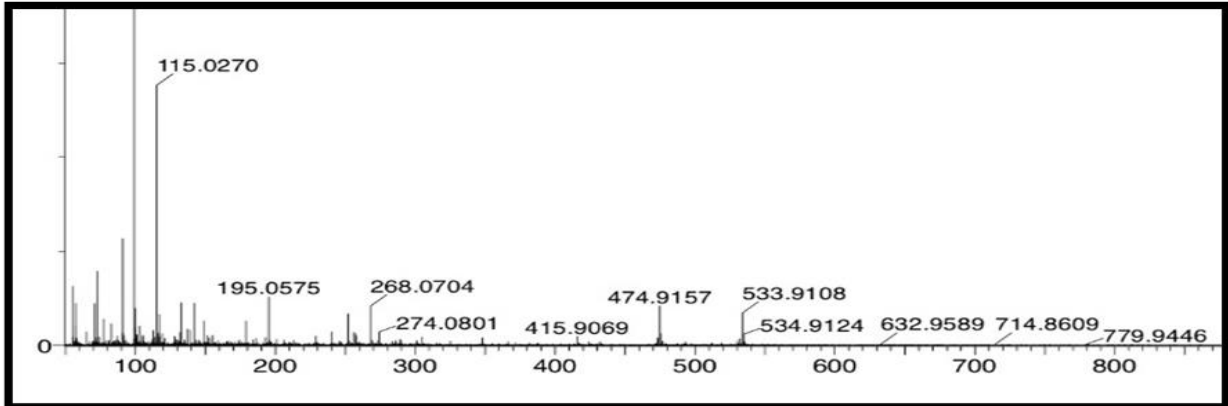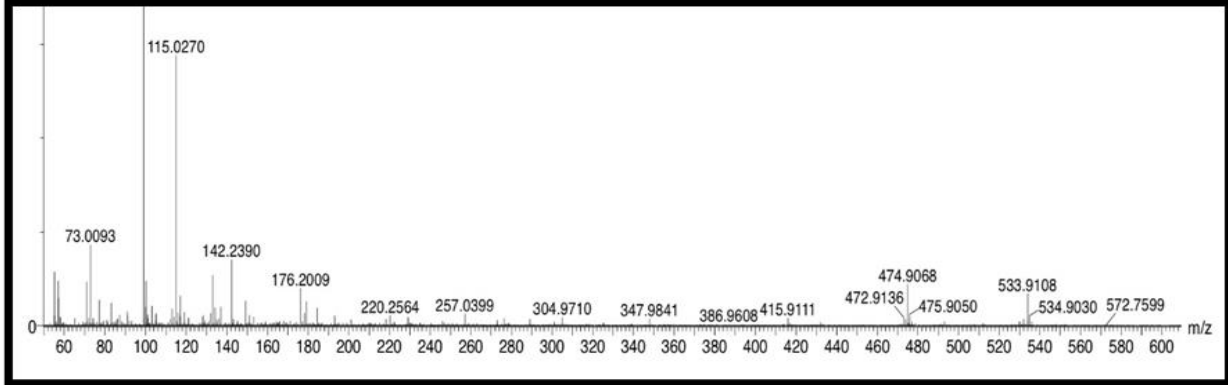
Sample drawn at 80 minutes
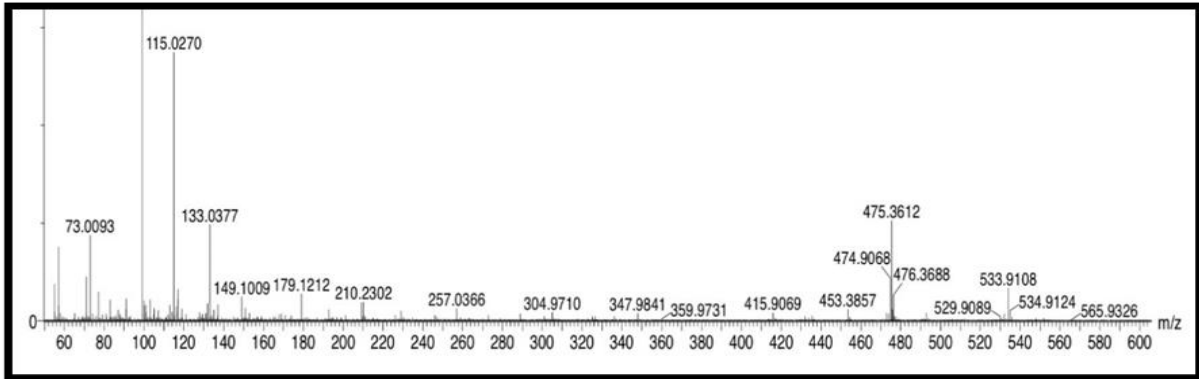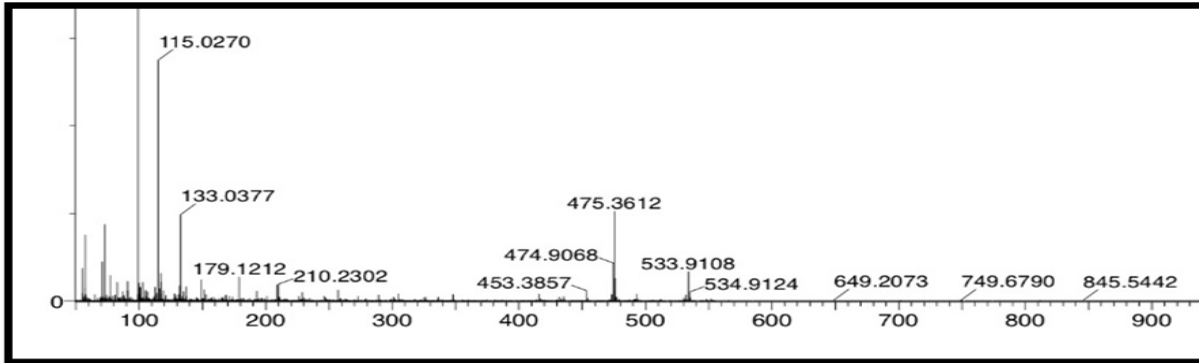
Sample drawn at 120 minutes
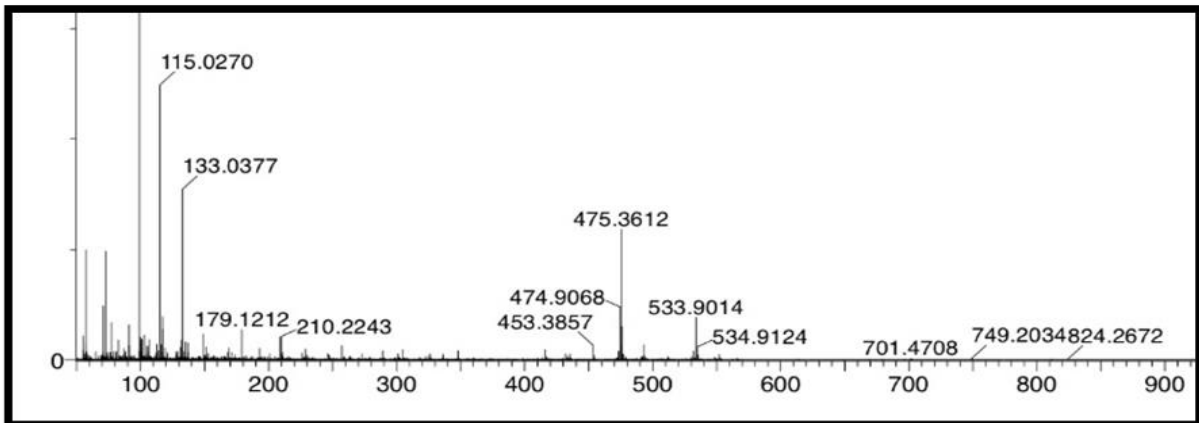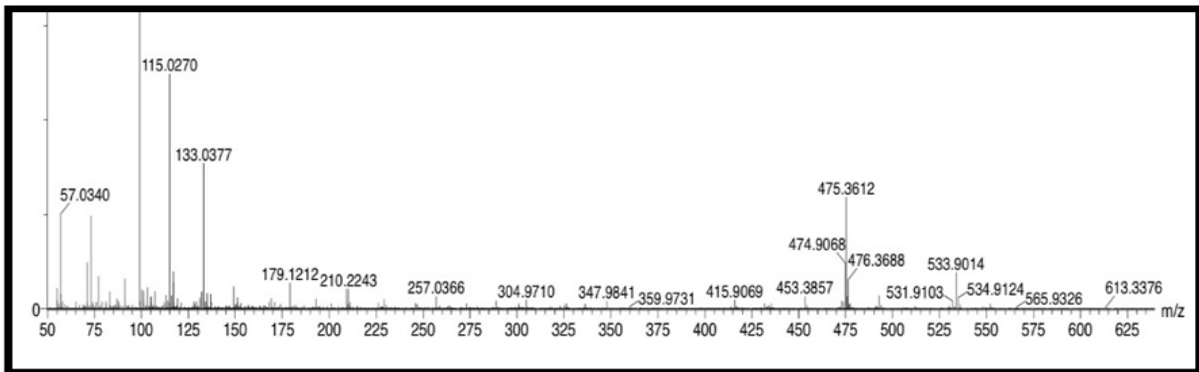
Sample drawn at 160 minutes
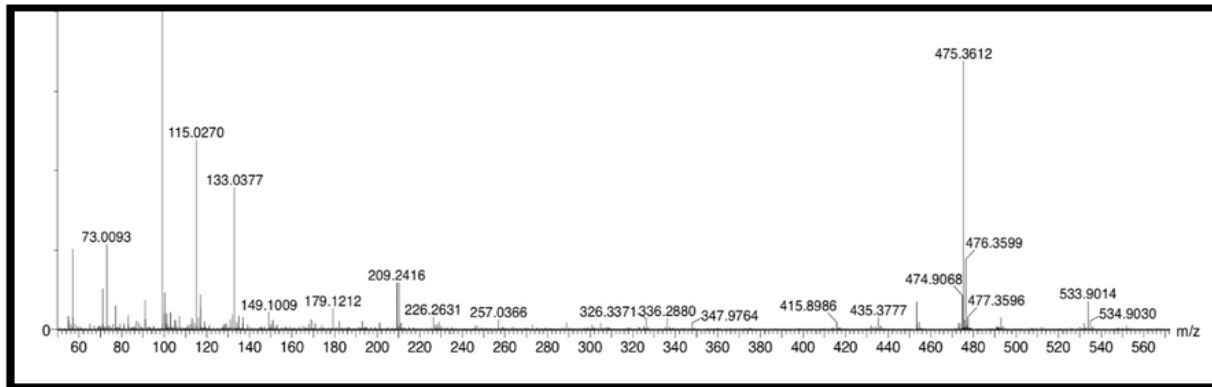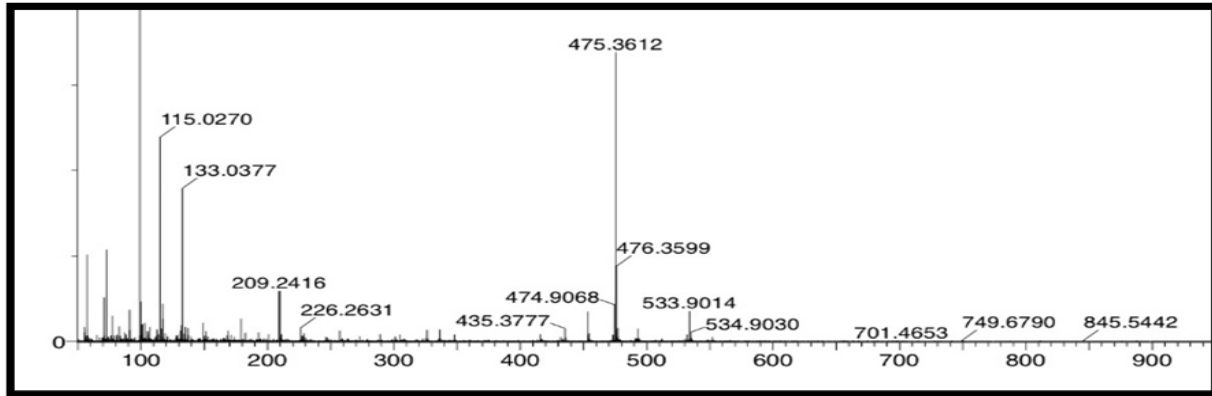
Sample drawn at 180 minutes (final)
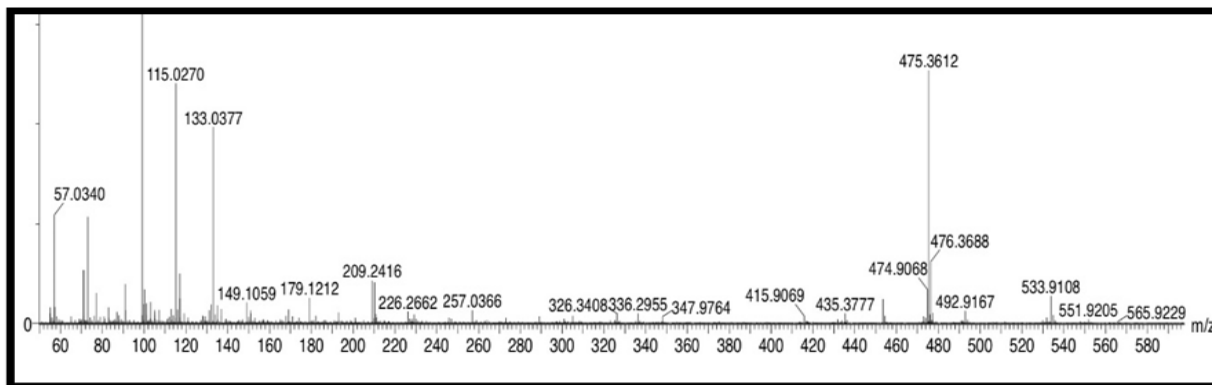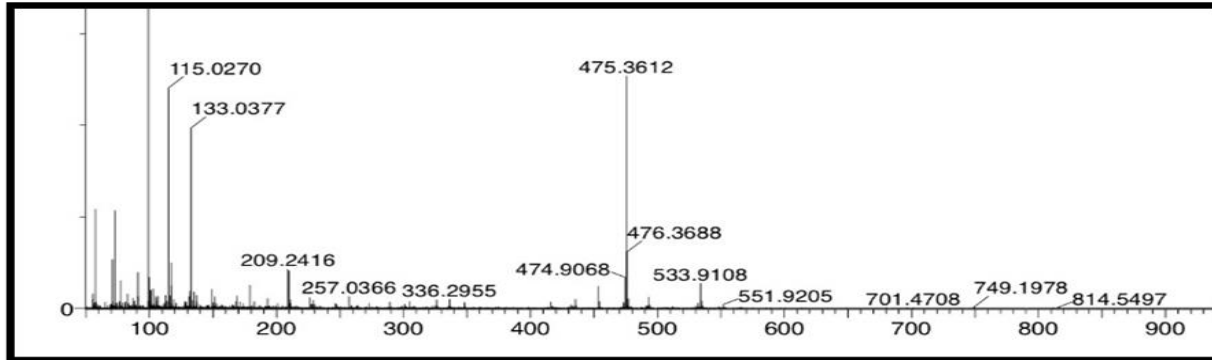
Figure 11: LCMS peaks for m/z values of different fragments to determine the degradation pathway

Abundant peaks observed in LCMS spectra were considered and a mechanistic pathway was determined for the degradation of erythrosine B dye. Molecular fragments with their actual and observed masses with the calculation of mass error are given in Table 2.

Table-2: Mass-to-charge ratio based on LC-MS/MS spectra during cleavage of Erythrosine B

Structure no.	Molecular Formula	m/z Exact Mass	m/z observed Mass	% Mass Error
A1	$C_{20}H_6I_4O_5$	-	834.88	-
A2	$C_{20}H_{10}I_4O_6$	845.54	852.89	0.99
A3	$C_{13}H_5I_4O_6$	749.68	749.79	1.00
A4	$C_7H_6O_3$	133.23	139.03	1.04
A5	$C_{13}H_5I_3O_5$	619.41	622.89	1.00
A6	$C_{13}H_{10}I_2O_7$	533.91	531.00	0.99
A7	$C_{12}H_8I_2O_4$	474.92	471.02	0.99
A8	$C_6H_5IO_4$	268.07	269.00	0.99
A8a	$C_6H_6O_4$	142.23	142.10	0.99
A8b	$C_3H_4O_2$	73.00	73.06	1.00
A8c	$C_3H_5IO_2$	201.12	200.98	0.99
A8d	$C_3H_5IO_2$	184.28	184.97	1.00
A8e	$C_4H_3IO_2$	210.23	210.97	1.00
A8f	C_3H_6O	59.13	59.08	0.99
A9	$C_6H_7IO_3$	243.36	243.01	0.99
A9a	$C_5H_8O_3$	115.02	116.1	1.00
A9b	$C_3H_5O_2$	73.00	74.06	1.01
A9c	C_2H_4O	45.07	45.05	0.99
A9d	$C_3H_6O_3$	91.13	91.07	0.99
A9e	$C_2H_2O_2$	59.13	59.04	0.99
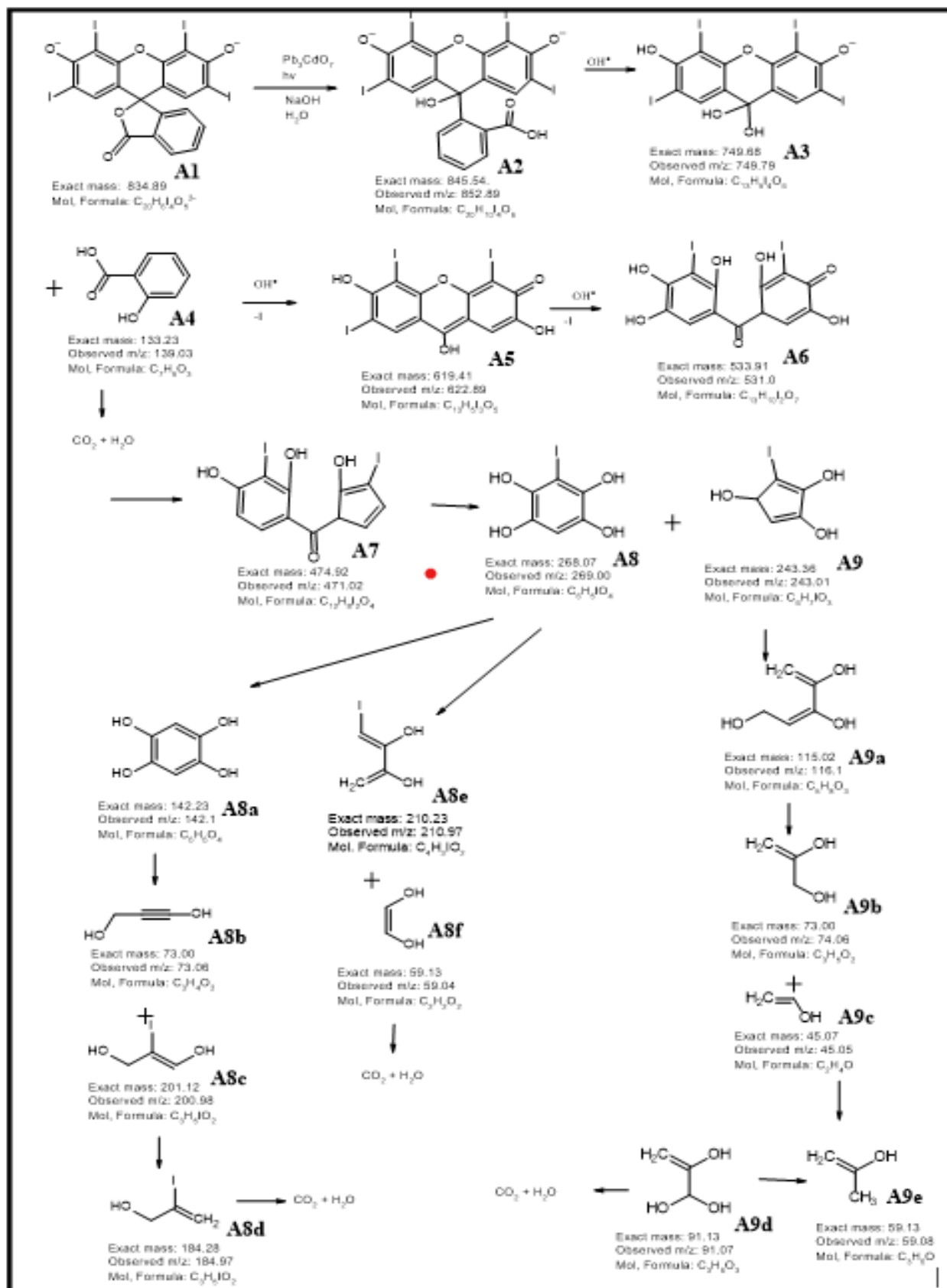
Figure 11 Shows a considerable decrease in the intensity of the peak of the parent molecule suggesting the gradual breakdown of it into fragments that are supported by new peak formation. Abundant peaks with different mass values are considered. It is observed that an attack of OH· free radical occurs on most steric carbon atoms breaking the bond and initiating the degradation process by forming molecules A3 and A4 having peaks at mass values of 749.79 and 139.03 which are endorsed by peaks in the LCMS graph. In the next step breakdown of conjugation and ring opening is shown by mass values of 619.41 in A5 and 533.91 in A6 molecules. Proceeding through A7 at a mass value of 471.02, fragmentation is observed forming two molecules A8 with a mass value of 269.0 and A9 with 243.36. Further following different routes and fragmentations, in the end, CO_2 and H_2O molecules are formed. Throughout the fragmentation, it was observed that the weaker bond site, that is most steric carbon atoms, is attacked by free radicals, and removal of conjugation is also evident.

IV. CONCLUSION

It is concluded here that the Pb_3CdO_7 nanocomposite is synthesized with 88% yield and characterized using various analytical techniques. Advanced characterization is carried out by DTA-TGA, PL, FL, and BET analyses. The particle size of Pb_3CdO_7 of 44.51 nm and band gap of 5.23 eV endorses that it is a nano composite and has the potential to function as a photocatalyst. Degradation rate-affecting variables are considered to analyze the photocatalytic efficiency of prepared nanocomposite by varying various factors. Further recycling test is carried out to check its reusability. A scavenger study is also done to rule out the mechanism. The degradation intermediates formed were determined by LCMS for erythrosine B dye and it was observed that it degrades completely into harmless smaller fragments like CO_2, H_2O etc. These findings showed that Pb_3CdO_7 nanocomposite can be used as a photocatalyst for the degradation of pollutants effectively and to make the environment clean at a very low cost by using natural energy sources. The quality of the water can thus be enhanced by this photocatalytic water treatment.

V. DECLARATION OF CONFLICTS OF INTEREST

The authors declare that they have no conflicts of interest.

VI. ACKNOWLEDGEMENT:

REFERENCES

[1] Nishanthi S T, Visible light photocatalytic degradation of environmental pollutants using metal oxide semiconductors, Photocat Func Mater env Rem, (2019) 41-67. https://doi.org/10.1002/9781119529941.ch2

[2] Lanjwani M F, Tuzen M, Khuhawar M Y & Saleh T A, Trends in photocatalytic degradation of organic dye pollutants using nanoparticles: a review, Inorg Chem Commun, 159 (2024) 111613. https://doi.org/10.1016/j.inoche.2023.111613

[3] Muhd Julkapli N, Bagheri S & Bee Abd Hamid S, Recent advances in heterogeneous photocatalytic decolorization of synthetic dyes, Sci World J, 1 (2014) 692307. doi: 10.1155/2014/692307

[4] Liu Z, Xu X, Fang J, Zhu X & Li B, Synergistic degradation of Eosin Y by photocatalysis and electrocatalysis in UV irradiated solution containing Hybrid $BiOCl/TiO_2$ particles, Water Air & Soil Pol, 223 (2012) 2783-2798. https://doi.org/10.1007/s11270-011-1066-4

[5] Gyawali G, Adhikari R, Joshi B, Kim T H, Rodríguez-González V & Lee S W, Sonochemical synthesis of solar-light-driven Ag-$PbMoO_4$ photocatalyst, J Hazard Mater, 263 (2013) 45-51. https://doi.org/10.1016/j.jhazmat.2013.03.065

[6] Sahu R K, Mohanta B S & Das N N, Synthesis, characterization, and photocatalytic activity of mixed oxides derived from ZnAlTi ternary layered double hydroxides, J Phy Chem Solids, 74(9) (2013) 1263-1270. https://doi.org/10.1016/j.jpcs.2013.04.002

[7] Xiang X, Xie L, Li Z & Li F, Ternary MgO/ZnO/In$_2$O$_3$ hetero-structured photocatalysts derived from a layered precursor and visible-light-induced photocatalytic activity, Chem Eng J, 221 (2013) 222-229. https://doi.org/10.1016/j.cej.2013.02.030

[8] Anchieta C G, Sallet D, Foletto E L, da Silva S S, Chiavone-Filho O, & do Nascimento C A, Synthesis of ternary zinc spinel oxides and their application in the photodegradation of organic pollutants, Ceram Int, 40(3) (2014) 4173-4178. https://doi.org/10.1016/j.ceramint.2013.08.074

[9] Ullah I, Ali S, Hanif M A & Zia M A, Synthesis and Photocatalytic Efficiency of Sunlight Driven Novel Ternary Metal Oxide Nanophotocatalyst, Asian J Chem, 27(4) (2015) 1189. https://doi.org/10.14233/ajchem.2015.17081

[10] Xu L, Wei Y, Guo W, Guo Y & Guo Y, One-pot solvothermal preparation and enhanced photocatalytic activity of metallic silver and graphene co-doped BiVO$_4$ ternary systems, Appl Surf Sci, 332 (2015) 682-693. https://doi.org/10.1016/j.apsusc.2015.01.235

[11] Kokane S B, Sartale S D, Girija K G & Sasikala R, Photocatalytic performance of Pd decorated TiO$_2$–CdO composite: Role of in situ formed CdS in the photocatalytic activity, Int J Hyd Eng, 40(39) (2015)13431-13442. https://doi.org/10.1016/j.ijhydene.2015.08.037

[12] Rauf A, Sher Shah M S A, Choi G H, Humayoun U B, Yoon D H, Bae J W & Yoo P J, Facile synthesis of hierarchically structured Bi$_2$S$_3$/Bi$_2$WO$_6$ photocatalysts for highly efficient reduction of Cr (VI), ACS Sustain Chem Eng, 3(11) (2015) 2847-2855. https://doi.org/10.1021/acssuschemeng.5b00783

[13] Vignesh S, Suganthi S, Sundar J K, Raj V & Devi P R I, Highly efficient visible light photocatalytic and antibacterial performance of PVP capped Cd: Ag: ZnO photocatalyst nanocomposites, Appl Surf Sci, 479 (2019) 914-929. https://doi.org/10.1016/j.apsusc.2019.02.064

[14] Preethi G, Balan R, Koppala S & Nagaswarupa H P, Cubic and orthorhombic Cd$_2$SnO$_4$ microcrystals: molten salt synthesis, phase evolution and dye degradation studies, Mater Res Exp, 6(10) (2019) 105537. DOI 10.1088/2053-1591/ab406f

[15] Harito C, Zaidi S Z, Bavykin D V, Martins A S, Yuliarto B, Walsh F C & de León C P, PbO$_2$ decorated ZnO-TiO$_2$ core-shell nanoflower structures by zinc anodizing for photo-and anodic degradation of Reactive Black-5 dye, Adv Nat Sci: Nanosc Nanotech, 11(3) (2020) 035018. DOI 10.1088/2043-6254/abb238

[16] Sirohi K, Kumar S, Singh V, Chauhan N & Vohra A, Synthesis, characterization and photocatalytic properties of graphene-CdO/SnO$_2$ ternary nanocomposites in visible light, Mater Res Exp, 6(7) (2019) 075901. DOI 10.1088/2053-1591/ab122c

[17] Munawar T, Yasmeen S, Hussain F, Mahmood K, Hussain A, Asghar M & Iqbal F, Synthesis of novel hetero-structured ZnO-CdO-CuO nanocomposite: characterization and enhanced sunlight driven photocatalytic activity, Mater Chem Phys, 249 (2020) 122983. https://doi.org/10.1016/j.matchemphys.2020.122983

[18] Munawar T, Iqbal F, Yasmeen S, Mahmood K & Hussain A, Multi metal oxide NiO-CdO-ZnO nanocomposite–synthesis, structural, optical, electrical properties and enhanced sunlight driven photocatalytic activity, Ceram Int, 46(2) (2020) 2421-2437. https://doi.org/10.1016/j.ceramint.2019.09.236

[19] Munawar Z, Ghazanfar S, Asif H M, Khan M A, Sirajuddin M, Tariq M & Haider A, Synthesis, characterization of ternary metal oxides nanocomposite (ZnO–CdO–Pr$_2$O$_3$) for photodegradation of organic pollutants: methylene blue & rhodamine B, J Iran Chem Soc, 20(9) (2023) 2245-2256. https://doi.org/10.1007/s13738-023-02824-8

[20] Moalej N S, Sheibani S & Mokmeli M, Ternary Z-scheme NiO/CdO/Co$_3$O$_4$ nanocomposite powder with enhanced photocatalytic activity under visible light irradiation, J Mater Sci: Mater Electron. 34(3) (2023) 195. https://doi.org/10.1007/s10854-022-09666-9

[21] Murugadoss G, Thiruppathi K, Venkatesh N, Hazra S, Mohankumar A, Thiruppathi G & Sakthivel P, Construction of novel quaternary nanocomposite and its synergistic effect towards superior photocatalytic and antibacterial application, J Environ Chem Eng, 10(1) (2022)

106961. https://doi.org/10.1016/j.jece.2021.106961

[22] Logambal S, Chandrasekar M, Kumar R A, Inmozhi C, Aravindan S, Uthrakumar R & Kaviyarasu K, Biosynthesis of PbO nanoparticles via Adhatoda vesica (Justicia adhatoda) leaves extract for antimicrobial and photocatalytic applications, J King Saud Univ-Sci, 36(5) (2024) 103169. https://doi.org/10.1016/j.jksus.2024.103169

[23] Asha S, Hentry C., Bindhu M R, Al-Mohaimeed A M, AbdelGawwad M R & Elshikh M S, improved photocatalytic activity for degradation of textile dyeing and wastewater and thiazine dyes using $PbWO_4$ nanoparticles synthesized by co-precipitation method, Env Res, 200 (2021) 111721. https://doi.org/10.1016/j.envres.2021.111721

[24] Karami M, Ghanbari M, Amiri O & Salavati-Niasari M, enhanced antibacterial activity and photocatalytic degradation of organic dyes under visible light using cesium lead iodide perovskite nanostructures prepared by hydrothermal method, Sep Pur Technol, **253** (2020) 117526.https://doi.org/10.1016/j.seppur.2020.117526

[25] Valian M, Salavati-Niasari M, Ganduh S H, Abdulsahib W K, Mahdi M A & Jasim L S, Sol-gel auto-combustion synthesis of a novel chitosan/$Ho_2Ti_2O_7$ nanocomposite and its characterization for photocatalytic degradation of organic pollutant in wastewater under visible illumination, Int J Hyd En, 47(49) (2022) 21146-21159. https://doi.org/10.1016/j.ijhydene.2022.04.221

[26] Arulkumar E, Shree S S & Thanikaikarasan S, Photocatalytic degradation efficiency of Rhodamine-B for CuO/CdO nanosheets attained through simple co-precipitation method, Results Chem, 6 (2023) 101169. https://doi.org/10.1016/j.rechem.2023.101169

[27] Monsef R, Soofivand F, Alshamsi H A, Al-Nayili A, Ghiyasiyan-Arani M & Salavati-Niasari M, Sonochemical synthesis and characterization of $PrVO_4$/CdO nanocomposite and their application as photocatalysts for removal of organic dyes in water, J Mol Liq, 336 (2021) 116339. https://doi.org/10.1016/j.molliq.2021.116339

[28] Warshagha M Z & Muneer M, Facile synthesis of CdO-ZnO heterojunction photocatalyst for rapid removal of organic contaminants from water using visible light, Env Nanotechnol Monitor Manag, 18 (2022)100728. https://doi.org/10.1016/j.enmm.2022.100728

[29] Khan S, Sadiq M & Muhammad N, Enhanced photocatalytic potential of TiO_2 nanoparticles in coupled $CdTiO_2$ and $ZnCdTiO_2$ nanocomposites, Env Sci Pol Res, 29(36) (2022) 54745-54755. https://doi.org/10.1007/s11356-022-19807-6

[30] Sirohi K, Kumar S, Singh V, Chauhan N & Vohra A, Facile synthesis of CdO–ZnO nanocomposites for photocatalytic application in visible light, Arab J Sci Eng, 49(1) (2024) 273-284. https://doi.org/10.1007/s13369-023-08072-5

[31] Kong L, Liu Y, Dong L, Zhang L, Qiao L, Wang W & You H, Enhanced red luminescence in $CaAl_{12}O_{19}$: Mn^{4+} via doping Ga^{3+} for plant growth lighting, J Dalton Trans, **49(6)** (2020) 1947-1954. DOI https://doi.org/10.1039/C9DT04086B

[32] Araújo V D, Tranquilin R L, Motta F V D, Paskocimas C A, Bernardi M I B, Cavalcante L S & Bomio M R D, Effect of polyvinyl alcohol on the shape, photoluminescence and photocatalytic properties of $PbMoO_4$ microcrystals, Mater Sci semicond Process, **26** (2014) 425-430.https://doi.org/10.1016/j.mssp.2014.05.027

[33] Nejati-Moghadam L, Gholamrezaei S, Salavati-Niasari M & Esmaeili-Bafghi-Karimabad A, Hydrothermal synthesis and characterization of lead oxide nanocrystal in presence of tetradentate Schiff-base and degradation investigation of organic pollutant in the wastewater, J Mater Sci: Mater Elect, **28** (2017) 9919-9926. doi:10.1007/s10854-017-6748-2

[34] Venkata Reddy C, Bandaru N, Shim J & Vattikuti S P, Synthesis of CdO/ZnS heterojunction for photodegradation of organic dye molecules, Appl Phys A, **123** (2017) 1-12. https://doi.org/10.1007/s00339-017-1013-3

[35] Liu F Y, Lin J H, Dai Y M, Chen L W, Huang S T, Yeh T W & Chen C C, Preparation of perovskites $PbBiO_2I$/PbO exhibiting visible-light photocatalytic activity, Catal Today, 314 (2018) 28-41. doi: 10.1016/j.cattod.2018.02.006

[36] Rahman M M, Asiri A M, Youssef T E & Marwani H M, Photocatalytic degradation of remazol brilliant orange 3R using wet-chemically prepared CdO-ZnO nanofibers for environmental remediation, Mater Exp, 6(2) (2016)137-148. doi:10.1166/mex.2016.1285

[37] Yu M, Li J, Sun W, Jiang M & Zhang F, Preparation, characterization, and photocatalytic properties of composite materials of copper (II) porphyrin/TiO_2, J Mater Sci, 49(16) (2014) 5519–5528. https://doi.org/10.1007/s10853-014-8132-4

[38] Prajapati D K, Chouhan J K, Menaria J, Tanwer T S & Bhardwaj S, Fabrication and characterization of photocatalyst Pb_3CdO_7 for degradation of Azure-A, J Environ St Poll Res, 10(1) (2024) 485-491. https://doi.org/10.30799/jespr.241.24100101